Thin Solid Films 615 (2016) 63–68

Contents lists available at ScienceDirect

Thin Solid Films

journal homepage: www.elsevier.com/locate/tsf

Deposition of silicon oxide coatings by atmospheric pressure plasma jet for oxygen diffusion barrier applications

Haitao Zhang, Zheng Guo, Qiang Chen, Xinwei Wang [1], Zhengduo Wang, Zhongwei Liu *

Beijing Institute of Graphic Communication, Beijing Key Laboratory of Printing and Packaging Materials and Technology, Laboratory of Plasma Physics and Materials, Beijing 102600, China

ARTICLE INFO

Article history:
Received 14 September 2015
Received in revised form 18 June 2016
Accepted 21 June 2016
Available online 25 June 2016

Keywords:
Atmospheric pressure
Barrier film
Plasma jet
Silicon oxide coatings

ABSTRACT

Silicon oxide thin-film coated polymer substrates have great applications in the packaging industry for food and medical products, because these types of treated substrates show excellent barrier properties toward oxygen and moisture diffusion. In this work, silicon oxide coatings were fabricated on polyethylene terephthalate and polyimide (PI) substrates by an atmospheric pressure jet. The deposited coatings have been carefully characterized by Fourier transform infrared spectroscopy, scanning electron microscope and atomic force microscope for chemical structures and morphology. The influence of the hexamethyldisiloxane concentration in feed gas and the distance from plasma nozzle to PI substrate is also carefully investigated. With optimized deposition conditions, the obtained silicon oxide coated PI substrates show a satisfactorily low oxygen transmission rate of 0.7 ml/m^2/day (at 25 °C, dry oxygen).

© 2016 Elsevier B.V. All rights reserved.

1. Introduction

Silicon oxide film coated polymer substrates have been used in a variety of industries, such as the food and pharmaceutical packaging industries, and the optical component and microelectronic manufacturing, since the silicon oxide is intrinsically hard, highly transparent with hydrophilic characteristics [1–3]. Many techniques have been developed to deposit silicon oxide coatings, including physical evaporation, magnetron sputtering, chemical vapor deposition (CVD), and plasma-enhanced chemical vapor deposition (PECVD) [4–13]. Among these available techniques, the atmospheric pressure PECVD is particularly desirable, because it can be operated without requiring complicated and expensive vacuum systems. Premkumar et al. [14] reported the first experimental study on silicon oxide coatings deposited in a roll-to-roll dielectric barrier discharge (DBD) reactor at atmospheric pressure. With 150 ppm tetraethyl orthosilicate in a gas mixture of N_2, Ar and O_2, the produced SiO_x films on polymeric substrate show excellent gas barrier performance towards O_2 presenting oxygen transmission rate (OTR) value of 5×10^{-3} ml/m^2/day, as the SiO_x thickness reaches 225 nm. Very recently, the same group investigated the moisture barrier performance of silica-like films as functions of dynamic deposition rate and substrate temperature [15]. Atmospheric pressure plasma jet (APPJ) is a source of non-equilibrium atmospheric pressure plasmas [16,17]. Compared to other types of the plasma systems, such as DBD, the jet system can be used not only for flat and thin substrates but also for large-scale three-dimensional structures, since the jet plasma is not confined between the electrodes and the dimension of the plasma can vary from several cm down to sub-mm region. Babayan et al. [18] reported that silica films can be produced by APPJ with the driving power from 40 to 500 W at 13.56 MHz radio frequency. Schäfer et al. [19] studied the influence of plasma parameters and jet geometry on the deposition profile, which can be varied from a ring pattern to a parabolic profile. Reuter et al. [5] investigated the role of oxygen in the surface reactions during the silicon oxide deposition process by APPJ. As the ratio of O_2 to hexamethyldisiloxane (HMDSO) increases, the silicon oxide growth rate also increases, along with which the HMDSO starts to show depletion behavior and form carbon free films. In these processes, the silicon oxide films were all deposited on the inflexible substrates, such as silicon or glass. For flexible substrates (e.g. polymers), only Lin et al. [20] reported using APPJ to grow organosilicon oxynitride ($SiO_xC_yN_z$) coatings on polycarbonate substrates, aiming to enhance the hardness of the substrate surface.

Polyethylene terephthalate (PET) polymers are widely used flexible materials in many fields ranging from food packing to microelectronics applications. Polyimide (PI) polymers are potential candidates for flexible substrates in devices such as foldable displays and integrated circuit smart card. However, these two kinds of polymers suffer from limited barrier properties against gas permeation, resulting in the short shelf lives or reduced device performance. The focus of the present work is to study the growth of silicon oxide coatings on flexible PET and PI to improve their gas barrier property by APPJ. The influences of the initial HMDSO concentration in the feed gas, as well as the substrate to jet nozzle distance on oxygen transmission rate have been explored.

* Corresponding author.
E-mail address: liuzhongwei@bigc.edu.cn (Z. Liu).
[1] School of Advanced Materials, Peking University Shenzhen Graduate School, Shenzhen 518055, China.

http://dx.doi.org/10.1016/j.tsf.2016.06.042
0040-6090/© 2016 Elsevier B.V. All rights reserved.

www.spm.com.cn

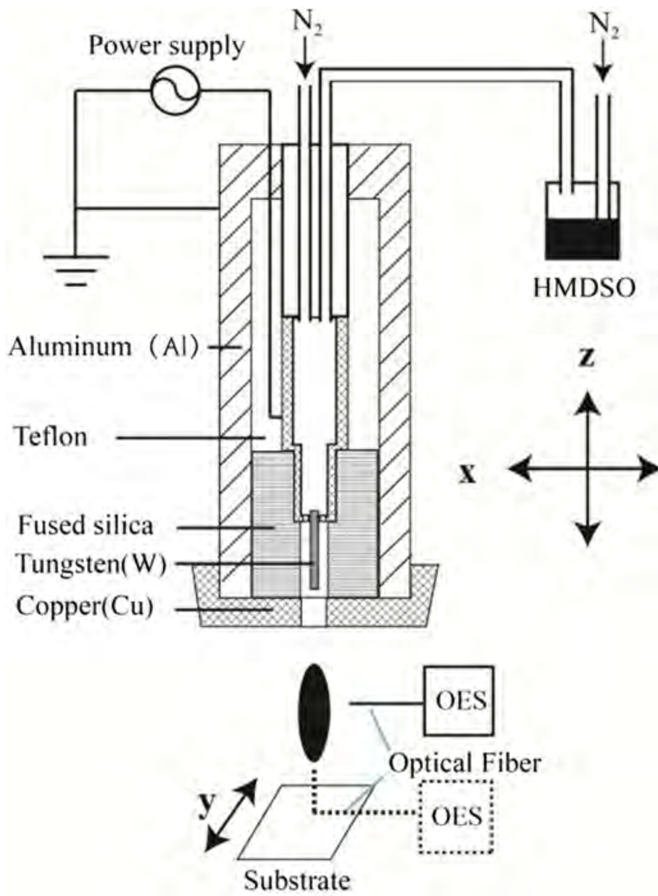

Fig. 1. Schematic diagram of the experimental setup.

2. Experimental

The experimental setup used in this work is schematically shown in Fig. 1. A tungsten needle electrode (1 mm diameter) was placed inside the aluminum tube (10 mm inner diameter, 26 mm outer diameter, 85 mm long). The lower end of the tube was covered by a copper cap with a pinhole of 1 mm in diameter to be used as the grounded electrode. A Teflon tube and a fused quartz tube were inserted between electrodes to make the discharge generated only in the region between the tungsten and the copper cap and the discharge gap is 3 mm. The centered tungsten electrode was driven by an excitation frequency (f_{ac}) of 21.4 kHz with 0–10 kV peak-to-peak voltage (U_p). The applied voltage and current were measured by a P6015A Tektronix high voltage probe and a 6021AC Tektronix current probe, respectively. The precursor of HMDSO for silicon oxide deposition was bubbled by mass-controlled N_2 carrier gas at ambient temperature, where the N_2 flow rate was varied from 100 to 500 standard cubic centimeters per minute (sccm). The discharge gas of high purity nitrogen (99.99%) flow was kept at 8 standard liters per minute (slm). HMDSO/N_2 and N_2 gases were premixed before entering the Teflon tube. The plasma jet was movable in x- and z-directions, and the substrate was moving along y-direction with the speed (S_c) of 0–1000 mm/min. Flexible PET and PI substrates (100 mm × 100 mm) were positioned on the substrate, which is 9–13 mm in distance (d) below the nozzle of the plasma jet. During silicon oxide deposition processes, the plasma jet scanned the polymeric substrates from one side to the other side in x-direction with a constant speed. When plasma jet crossed either side of the polymeric substrate, the substrate moved a small step in y direction. The jet and substrate repeated the above movements until the whole polymeric substrate was scanned. The gas temperature is a critical factor to consider for the deposition. To measure the gas temperature, a K-type (Ni–Cr/Ni–Al) thermocouple was inserted along the symmetric axis of the torch. Unless otherwise stated, standard processing conditions (3228 ppm HMDSO, S_c = 400 mm/min, d = 11 mm, f_{ac} = 21.4 kHz, U_p = 2.9 kV,) were used in this work.

To collect the plasma emission spectra between the high voltage and grounded electrodes, the spectrometer (AvaSpec Multichannel Fiber Optic Spectrometer, range 190–900 nm, resolution 0.07 nm at 600 nm) was equipped with five 75 mm focal length spectrometer channels. All of the channels consist of 2048 pixel CCD detectors and holographic diffraction gratings of 1800 grooves/mm with 10 μm slits. The UV-transparent optical fiber was mounted facing the entrance of APPJ, which was 20 cm away from the nozzle. To measure the optical emission of the plasma jet effluents, the optical fiber was placed 10 mm away from the nozzle, perpendicularly to the jet flow, and mounted on a stand that can slide along the plasma axis to perform a scan.

The thickness of the deposited silicon oxide coatings was measured by a surface profilometer (Dektak 150 Veeco Inc.). The chemical structure of the coatings was analyzed by a Fourier transform infrared (FTIR) spectrometer (Nicolet 6700 Thermo Sci. Inc.). All FTIR spectra were recorded for 32 scans in the spectral range between 400 and 4000 cm^{-1} with 4 cm^{-1} resolution. The film composition was ensured by X-ray photoelectron spectroscopy (XPS) using monochromated Al Kα radiation (Thermo Scientific, Escalab 250Xi). The pass energies for survey and high-resolution scans were 50 and 20 eV, respectively. To remove the adventitious carbon on sample surface, 30 s of 2 keV Ar^+ sputtering was performed. Film surface morphology was examined by scanning electron microscopy (SEM, SU8020 Hitachi Inc.) at 15 kV and atomic force microscopy (AFM, CSPM3000, BenYuan China) in contact mode. The topography images and the corresponding average surface roughness were collected. To measure OTR, an oxygen permeation analyzer (8001, Illinois Inc.) was used to measure the prepared samples with size of 100 cm^2.

www.spm.com.cn

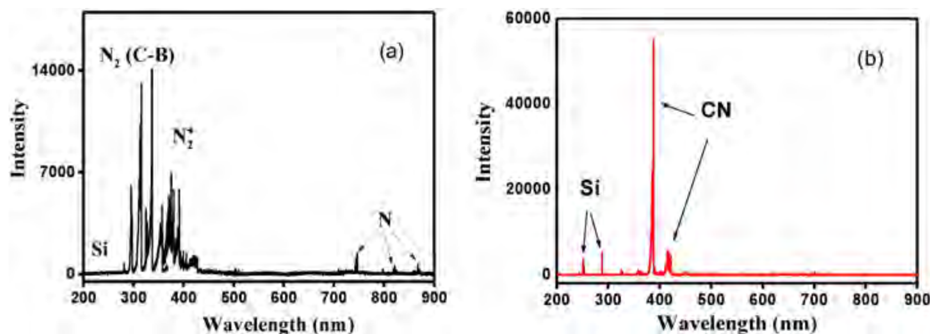

Fig. 2. Optical emission spectra of HMDSO/N_2 plasma for the optical fiber placed (a) facing plasma nozzle; (b) at the side of plasma jet effluent (3228 ppm HMDSO, S_c = 400 mm/min, d = 11 mm, f_{ac} = 21.4 kHz, U_p = 2.9 kV).

3. Results and discussion

Fig. 2 shows typical optical spectra of HMDSO/N_2 in APPJ with applied voltage U_p = 2.9 kV, N_2 flow rate F_{N2} = 8 slm, and N_2 carrier gas flow rate F_{N2} = 500 sccm which corresponds to the HMDSO concentration of 3228 ppm. When the optical fiber was positioned facing the plasma nozzle, the emission spectrum (Fig. 2(a)) includes mainly the emissions from N_2 ($C^3\Pi_u$), CN (B), and N_2^+ ($B^2\Sigma_u^+$), as well as some atomic lines from N and Si. The side-view optical emission spectrum of plasma jet is shown in Fig. 2(b), where the emissions from CN and Si were dominating.

In atmospheric pressure HMDSO/N_2 plasma (3228 ppm HMDSO in N_2), electrons are accelerated to have high kinetic energy by the electric field. The inelastic collisions of the energetic electrons with the ambient N_2 molecules can generate many excited nitrogen molecules. As Ding et al. [21] pointed out, in the atmospheric pressure N_2 plasma, aside from the vibrational excitations with the electrons in their ground state, the first electronic excitation state of molecular nitrogen N_2 ($A^3\Sigma_u^+$) can also play an important role in initiating numerous plasma processes. The rate coefficient to generate N_2 ($A^3\Sigma_u^+$) via the collisions between electrons and nitrogen molecules is as high as 1.1×10^{-10} cm^3 molecule^{-1} s^{-1} and its radiative lifetime is about 2 s. Since the energy of the N_2 ($A^3\Sigma_u^+$) species is about 6.2 eV above the ground state, which is much higher than Si—C bond (~3.3 eV), Si—O bond (~4.8 eV), O—H bond (~4.8 eV) and O—O bond (~1.5 eV), the N_2 ($A^3\Sigma_u^+$) species is capable to dissociate HMDSO, O_2 and H_2O molecules.

Unlike the plasma region between two electrodes, the effluent region should be free of electrons and charged particles. Thus, excited N_2 molecules cannot be generated in the effluent region as in the plasma region. On the other hand, the exited species left from the plasma region will react with the ambient O_2 and H_2O to form reactive O and OH species, which are considered as the oxygen source for silicon oxide formation [22,23].

The main physico-chemical processes in the HMDSO/N_2 discharge are summarized in Table 1. Reactions 1–3 are the primary collision processes between electrons and nitrogen molecules. Since for typical atmospheric pressure local thermal plasma, the mean electron energy, $\langle E_e \rangle$, is about 3–4 eV [24], the rate constants associated with $\langle E_e \rangle = 3$ eV are listed in Table 1. The processes 4–9 are related to the reactions of the excited and radical species with HMDSO, and the resulting products are Si and Si-containing species. Reactions 10 and 11 deal with the reactions of atomic Si and Si-containing species with O_2. Direct interaction between the electrons and HMDSO can be safely ignored because of their small concentrations in the plasma.

With the standard processing conditions (3228 ppm HMDSO, S_c = 400 mm/min, d = 11 mm, f_{ac} = 21.4 kHz, U_p = 2.9 kV), the silicon oxide coatings were grown on the polymeric substrates. To exclude the influence of the organic bonds from the PI and PET substrates, controlled experiments were also carried out on flat potassium bromide (KBr) tablets. Typical FTIR spectra with different initial HMDSO concentrations in the feed gas are plotted in Fig. 3. The coatings are characterized by strong absorption bands at 1070 cm^{-1}, 1180 cm^{-1} and 805 cm^{-1}. Luna-Lopez et al. [30] reported the Si–O–Si asymmetric stretching absorption band at 1082 cm^{-1} and bending vibration at 812 cm^{-1} in stoichiometric thermal SiO_2 films. Similarly, Lin et al. [20] reported the region 1005–1070 cm^{-1} can be used as a gauge for the portion of oxygen-rich inorganic SiO_x films with $1 \le x \le 2$. In this study, the peaks at 1070 cm^{-1}, 1180 cm^{-1} and 805 cm^{-1} can be assigned to the Si–O–Si asymmetric stretching, symmetric stretching band and bending vibration, which close to those in stoichiometric thermal SiO_2 films. Fig. 3(c) and (d) clearly shows the absorption bands at 926 cm^{-1} and in the region 3100–3700 cm^{-1} which can be attributed to Si—OH and O—H bonds, while the weak peaks at 1650 cm^{-1} corresponds to incorporation of water in the film. With the increase of the carrier gas flow from 100 sccm to 500 sccm, which corresponds to the

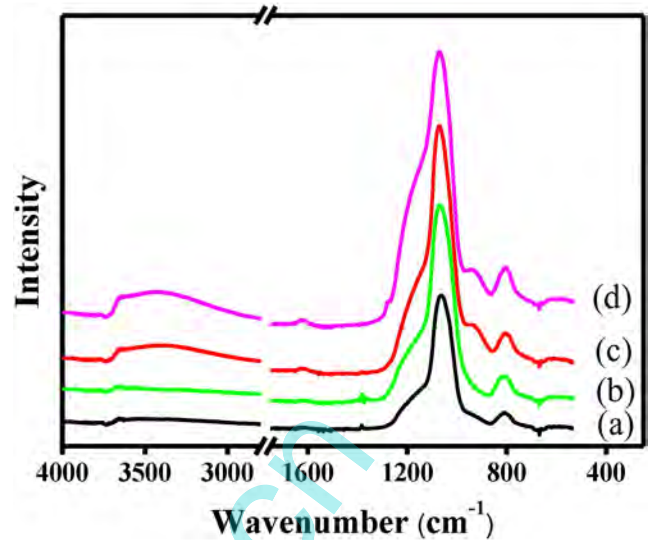

Fig. 3. Typical FTIR spectra of silicon oxide coatings on KBr versus HMDSO concentrations (a) 677 ppm; (b) 1338 ppm; (c) 1983 ppm; (d) 3228 ppm (S_c = 400 mm/min, d = 11 mm, f_{ac} = 21.4 kHz, U_p = 2.9 kV).

Table 1
Summary of the main elemental reactions in HMDSO/ N_2 plasma.

No.	Reaction	Rate coefficient k[a] [cm^3 molecule^{-1} s^{-1}]	Ref.
1	$e + N_2 (\upsilon = 0) \rightarrow e + N_2 (\upsilon = 1\text{–}10)$		
2	$\rightarrow e + N_2 (A^3\Sigma_u^+)$	1.1×10^{-10}	[25]
3	$\rightarrow e + N + N$		
4	$N_2 (A^3\Sigma_u^+) + (CH_3)_3SiOSi(CH_3)_3 \rightarrow N_2 + Si_xO_yC_zH_t$		
5	$N_2 (A^3\Sigma_u^+) + H_2O \rightarrow OH + H + N_2$	5×10^{-14}	[26]
6	$N_2 (A^3\Sigma_u^+) + O_2 \rightarrow N_2 + 2O$	2.5×10^{-12}	[26]
7	$O + (CH_3)_3SiOSi(CH_3)_3 \rightarrow (CH_3)_3SiOSiO(CH_3) + 2\,CH_3$		[27]
8	$O_2 + (CH_3)_3SiOSi(CH_3)_3 \rightarrow (CH_3)_3SiOSiO(CH_3) + CH_3OH + CH_3$		[27]
9	$OH + (CH_3)_3SiOSi(CH_3)_3 \rightarrow Si_xO_yC_zH_t$	1.38×10^{-12}	[28]
10	$Si_xO_yC_zH_t + O_2 \rightarrow$ products		
11	$Si + O_2 \rightarrow$ products	2.71×10^{-10}	[29]

[a] (1) For electron-involved processes, the mean electron energy $< E_e > = 3$ eV. (2) For bimolecular processes, the gas temperature T_g = 293 K.

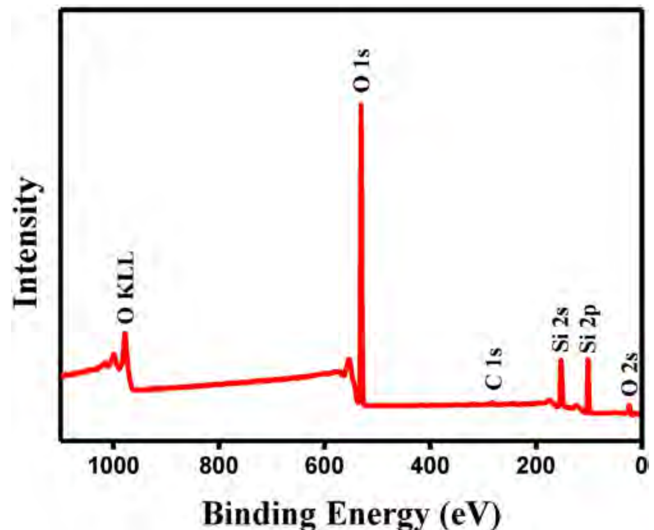

Fig. 4. XPS spectrum of the deposited film (3228 ppm HMDSO, S_c = 400 mm/min, d = 11 mm, f_{ac} = 21.4 kHz, U_p = 2.9 kV).

www.spm.com.cn

content of HMDSO in the feed mixture increased from 677 ppm to 3228 ppm, the Si-O-Si stretching band became stronger and broader. There were no obvious Si–CH_3 absorption bands at 1260–1270 cm^{-1} in Fig. 3, which indicates that the carbon content in the silicon oxide coatings was very low. Base on the above results and analysis, we conclude that the deposited films are oxygen-rich inorganic films which are also consistent with the XPS measurements as will be shown later.

The film composition was examined by XPS. After 30 s of Ar^+ sputtering for removing the surface adventitious carbon, only silicon, oxygen and carbon peaks were observed (Fig. 4), showing an atomic composition of $SiO_{1.4}C_{0.03}$. The low carbon content is in good agreement with FTIR measurements. There are two types of possible carbon-loss reactions in the deposition process of silicon oxide coatings. One is that HMDSO and $Si_xO_yC_zH_t$ react with the reactive species such as O and O_2 via R7, R8 and R10 to produce the volatile carbon-containing products; the other is the surface reactions of excited N_2 ($A^3\Sigma_u^+$) to remove carbon from the growing films, as pointed out by Reuter et al. [31,32].

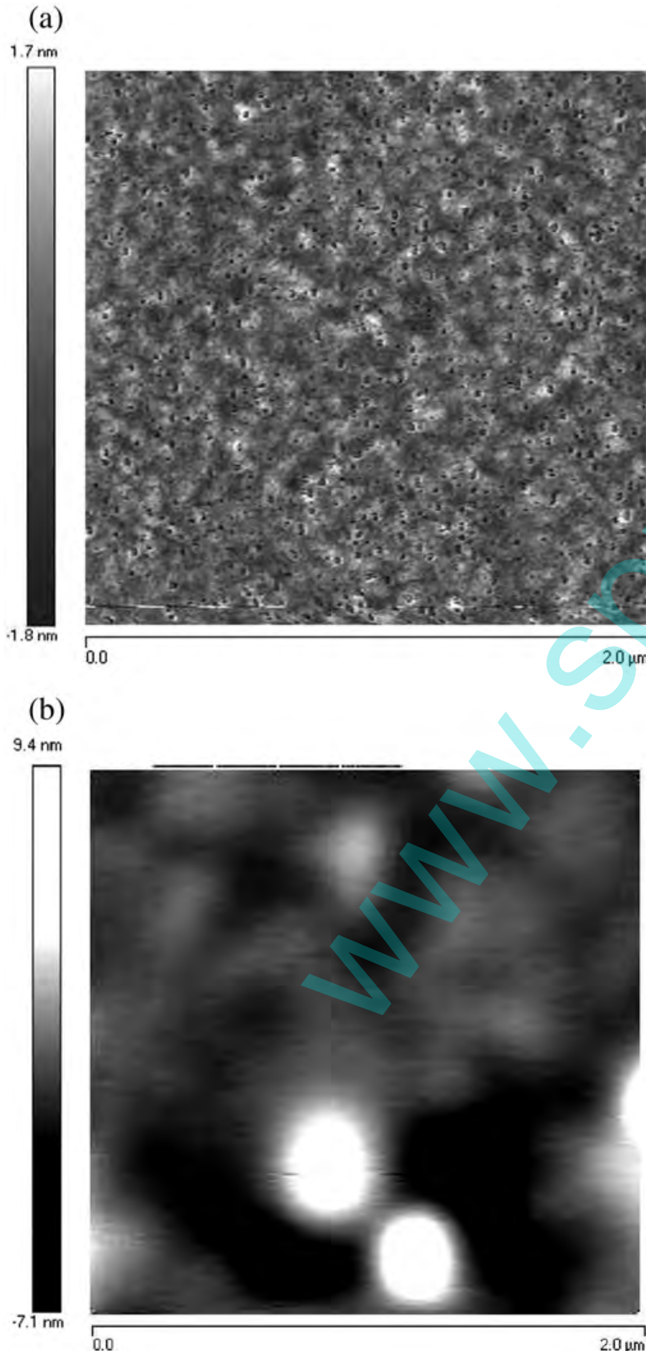

Fig. 5. AFM images of (a) bare PI substrate and (b) silicon oxide coatings (3228 ppm HMDSO, S_c = 400 mm/min, d = 11 mm, f_{ac} = 21.4 kHz, U_p = 2.9 kV).

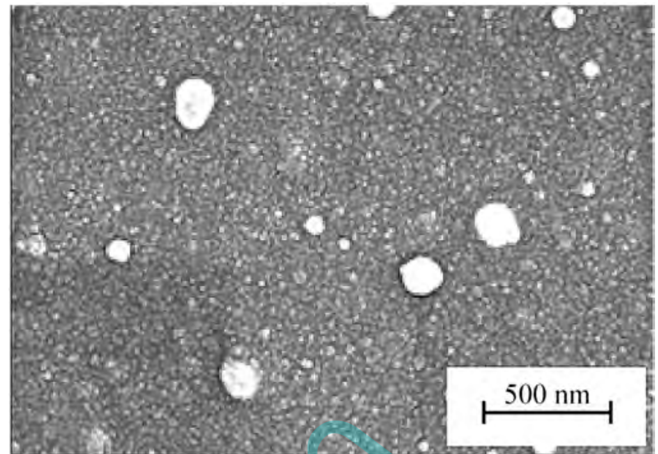

Fig. 6. SEM image of silicon oxide coated PI substrate (3228 ppm HMDSO, S_c = 400 mm/min, d = 11 mm, f_{ac} = 21.4 kHz, U_p = 2.9 kV).

Microstructure and morphology of the silicon oxide films are correlated to the coating barrier properties. Kim et al. and Howells et al. [8,33] reported that the barrier properties of the deposited coatings on the polymer substrates were affected by the surface morphology. Fig. 5 shows the AFM images of a bare PI substrate and a silicon oxide coated substrate. The bare PI had a smooth surface with the average roughness, R_a, of 0.36 nm. After the silicon oxide deposition by APPJ, R_a increased to 1.17 nm. The morphology of the silicon oxide coating, as shown in Fig. 5(b), shows many densely-packed small grains with well-defined grain boundaries. From the SEM micrograph shown in Fig. 6, the deposited silicon oxide is found to coat the substrate conformally. However, if we looked into the details of Fig. 6 carefully, it can be found that a minimum of pinhole and other large-scale defects (from 60 nm to 150 nm in diameter), which very likely come from the reactive nature of PECVD gases, chemical inhomogeneities on the surface and dust particles formed in the plasma [34,35].

The influences of the initial HMDSO concentration in the feed gas on the film thickness and permeation properties towards oxygen are shown in Fig. 7. As the HMDSO concentration increases, the film thickness (growth rate) increases, and both oxygen diffusion barrier properties of silicon oxide coatings deposited on PET and PI are also improved.

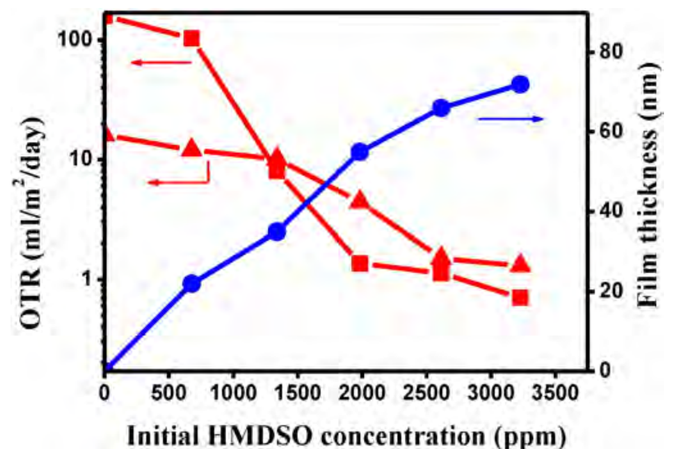

Fig. 7. OTR data and film thickness versus HMDSO concentration (■ on PI, ▲ on PET, S_c = 400 mm/min, d = 11 mm, f_{ac} = 21.4 kHz, U_p = 2.9 kV).

www.spm.com.cn

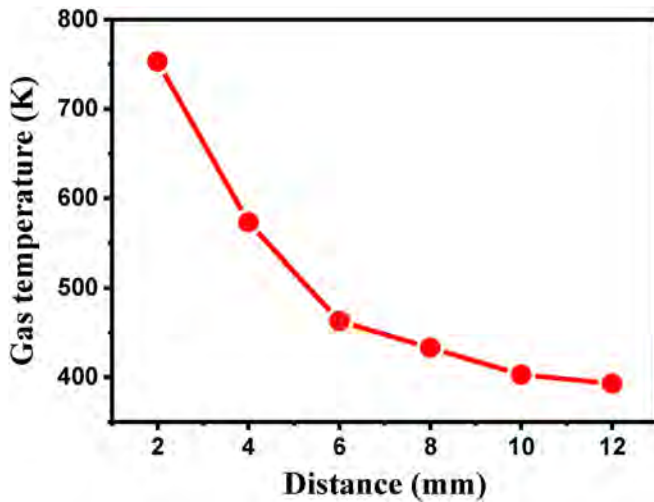

Fig. 8. Gas temperature in effluent region with respect to the substrate-to-nozzle distance (3228 ppm HMDSO, $S_c = 400$ mm/min, $f_{ac} = 21.4$ kHz, $U_p = 2.9$ kV).

The positive effect of HMDSO can be attributed to the $Si_xO_yC_zH_t$ species generated from the reactions of HMDSO with N_2 ($A^3\Sigma_u^+$), O_2, O and OH in reactions 7–9, because these species can enhance the silicon oxide production via reactions 10 and 11.

In our experiments, as shown in Fig. 7, the OTR values decrease sharply from 160 ml/m^2/day to 0.7 ml/m^2/day on PI substrates, and from 16 ml/m^2/day to 1.3 ml/m^2/day on PET substrates, as HMDSO concentration increases from 0 to 3328 ppm. It has to be pointed out that the silicon oxide coatings deposited by physical vapor deposition or chemical vapor deposition usually contain a large amount of defects, such as pinholes, pores, microchannels/microcracks, and/or grain boundaries, resulting in the gas permeation to occur easily through these defects, as Chatham and Roberts et al. reported [36,37]. It is very likely that the defect density in the deposited coatings decreases as the film thickness increases. As a result, the improvement of oxygen barrier performance of the deposited silicon oxide film is proportional to the layer thickness.

As shown in Fig. 8, inside the torch there was a drastic temperature change with respect to the distance to the plasma jet nozzle. As the distance (d) increased from 2 mm to 12 mm, the gas temperature deceased quickly from 753 K to 393 K. Fig. 9 shows the film thickness and oxygen transmission rate of the deposited silicon oxide films on PI substrates with respect to the distance. The monotonous decrease of film thickness can be ascribed to the decay of the highly reactive species via reactions

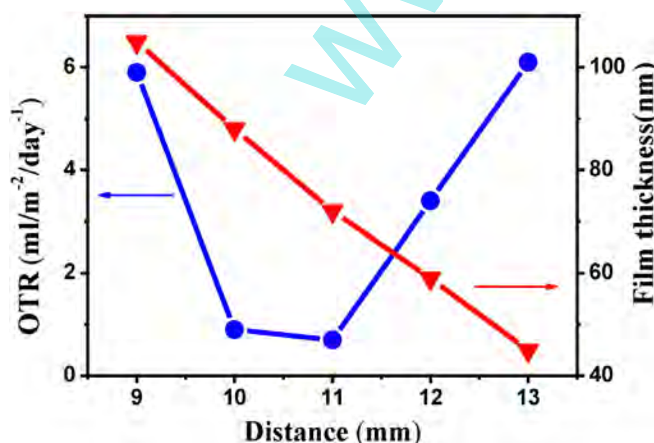

Fig. 9. OTR and coating thickness with respect to the substrate-to-nozzle distance (3228 ppm HMDSO, $S_c = 400$ mm/min, $f_{ac} = 21.4$ kHz, $U_p = 2.9$ kV).

4–9. Moreover, the geometrical spreading of the gas flow can also dilute the concentrations of the reactive species and result in the film thickness to decrease, as reported by Lommatzsch et al. [1]. As for the barrier properties of silicon oxide films, there is an optimal value of the substrate-to-nozzle distance for the OTR to achieve its minimum, i.e. $d = 11$ mm in our case. This is because, if the PI substrate is placed too close to the nozzle, the high temperature gas can damage the PI substrate, but if the PI substrate is placed too far, the deposited silicon oxide coating is too thin to block the oxygen permeation.

4. Conclusion

Atmospheric pressure plasma jet has been applied to deposit silicon oxide thin coatings on PET and PI substrates for gas diffusion barrier applications. The silicon oxide coatings were deposited from HMDSO and nitrogen mixture. At certain discharge condition (ac frequency of 21.4 kHz, applied voltage of 2.9 kV, APPJ scan speed of 400 mm/min, and PI substrate distance of 11 mm) the OTR value decreased sharply to only 0.7 ml/m^2/day, with increasing the HMDSO concentration to 3228 ppm. The barrier property as a function of the nozzle/substrate distance has also been investigated.

Acknowledgments

This work is financially supported by NSFC (Grant No. 11375031, 51302007), BMNSF (Grant No. 4162024), the Importation and Development of High-Caliber Talents Project of Beijing Municipal Institutions (Grant No. CIT&TCD201404130, KM201510015002), Guangdong Natural Science Funds for Distinguished Young Scholar (Grant No. 2015 A030306036), Shenzhen Science and Technology Innovation Committee (Grant No. KQCX20150327093155293) and State Key Laboratory of Electrical Insulation and Power Equipment (Grant No. EIPE15208).

References

[1] U. Lommatzsch, J. Ihde, Plasma polymerization of HMDSO with an atmospheric pressure plasma jet for corrosion protection of aluminum and low-adhesion surfaces, Plasma Process. Polym. 6 (2009) 642–648.
[2] F. Fei, Z. Wang, Q. Chen, Z. Liu, L. Sang, Study of functional barrier layer on PVC by PECVD for migrations resistant, Surf. Coat. Technol. 228 (Supplement 1) (2013) S61–S66.
[3] L. Zajíčková, V. Buršíková, V. Peřina, A. Macková, D. Subedi, J. Janča, S. Smirnov, Plasma modification of polycarbonates, Surf. Coat. Technol. 142–144 (2001) 449–454.
[4] B. Mailhot, A. Rivaton, J.-L. Gardette, A. Moustaghfir, E. Tomasella, M. Jacquet, X.-G. Ma, K. Komvopoulos, Enhancement of the photoprotection and nanomechanical properties of polycarbonate by deposition of thin ceramic coatings, J. Appl. Phys. 99 (2006) 104310.
[5] R. Reuter, K. Rügner, D. Ellerweg, T. de los Arcos, A. von Keudell, J. Benedikt, The role of oxygen and surface reactions in the deposition of silicon oxide like films from HMDSO at atmospheric pressure, Plasma Process. Polym. 9 (2012) 1116–1124.
[6] R. Morent, N. De Geyter, S. Van Vlierberghe, P. Dubruel, C. Leys, E. Schacht, Organic–inorganic behaviour of HMDSO films plasma-polymerized at atmospheric pressure, Surf. Coat. Technol. 203 (2009) 1366–1372.
[7] D. Hiller, R. Zierold, J. Bachmann, M. Alexe, Y. Yang, J.W. Gerlach, A. Stesmans, M. Jivanescu, U. Müller, J. Vogt, H. Hilmer, P. Löper, M. Künle, F. Munnik, K. Nielsch, M. Zacharias, Low temperature silicon dioxide by thermal atomic layer deposition: investigation of material properties, J. Appl. Phys. 107 (2010) 064314.
[8] S.-R. Kim, M.H. Choudhury, W.-H. Kim, G.-H. Kim, Effects of argon and oxygen flow rate on water vapor barrier properties of silicon oxide coatings deposited on polyethylene terephthalate by plasma enhanced chemical vapor deposition, Thin Solid Films 518 (2010) 1929–1934.
[9] T.W. Kim, M. Yan, G. Erlat, P.A. McConnelee, M. Pellow, J. Deluca, T.P. Feist, A.R. Duggal, M. Schaepkens, Transparent hybrid inorganic/organic barrier coatings for plastic organic light-emitting diode substrates, J. Vac. Sci. Technol. A 23 (2005) 971–977.
[10] P.A. Premkumar, S.A. Starostin, H. de Vries, R.M.J. Paffen, M. Creatore, T.J. Eijkemans, P.M. Koenraad, M.C.M. van de Sanden, High quality SiO2-like layers by large area atmospheric pressure plasma enhanced CVD: deposition process studies by surface analysis, Plasma Process. Polym. 6 (2009) 693–702.
[11] L. Seunghun, K. Yong-Jin, J. Sunghoon, K. Jong-Kuk, K. Do-Geun, Plasma-deposited SiOxCyHz barrier coatings for organic device encapsulation, Jpn. J. Appl. Phys. 52 (2013) 076001.
[12] A.S.D. Sobrinho, N. Schuhler, J.E. Klemberg-Sapieha, M.R. Wertheimer, M. Andrews, S.C. Gujrathi, Plasma-deposited silicon oxide and silicon nitride films on poly(ethylene terephthalate): a multitechnique study of the interphase regions, J. Vac. Sci. Technol. A 16 (1998) 2021–2030.

www.spm.com.cn

[13] S. Steves, B. Ozkaya, C.N. Liu, O. Ozcan, N. Bibinov, G. Grundmeier, P. Awakowicz, Silicon oxide barrier films deposited on PET foils in pulsed plasmas: influence of substrate bias on deposition process and film properties, J. Phys. D. Appl. Phys. 46 (2013) 084013.
[14] P.A. Premkumar, S.A. Starostin, M. Creatore, H. de Vries, R.M.J. Paffen, P.M. Koenraad, M.C.M. van de Sanden, Smooth and self-similar SiO2-like films on polymers synthesized in roll-to-roll atmospheric pressure-PECVD for gas diffusion barrier applications, Plasma Process. Polym. 7 (2010) 635–639.
[15] S.A. Starostin, M. Creatore, J.B. Bouwstra, M.C.M. van de Sanden, H.W. de Vries, Towards roll-to-roll deposition of high quality moisture barrier films on polymers by atmospheric pressure plasma assisted process, Plasma Process. Polym. 12 (2015) 545–554.
[16] U. Lommatzsch, D. Pasedag, A. Baalmann, G. Ellinghorst, H.-E. Wagner, Atmospheric pressure plasma jet treatment of polyethylene surfaces for adhesion improvement, Plasma Process. Polym. 4 (2007) S1041–S1045.
[17] M. Babij, Z.W. Kowalski, K. Nitsch, J. Silberring, T. Gotszalk, Atmospheric pressure plasma jet with high-voltage power supply based on piezoelectric transformer, Rev. Sci. Instrum. 85 (2014) 054703.
[18] S.E. Babayan, J.Y. Jeong, V.J. Tu, J. Park, G.S. Selwyn, R.F. Hicks, Deposition of silicon dioxide films with an atmospheric-pressure plasma jet, Plasma Sources Sci. Technol. 7 (1998) 286.
[19] J. Schäfer, R. Foest, A. Quade, A. Ohl, K.D. Weltmann, Local deposition of SiOx plasma polymer films by a miniaturized atmospheric pressure plasma jet (APPJ), J. Phys. D. Appl. Phys. 41 (2008) 194010.
[20] Y.-S. Lin, M.-S. Weng, T.-W. Chung, C. Huang, Enhanced surface hardness of flexible polycarbonate substrates using plasma-polymerized organosilicon oxynitride films by air plasma jet under atmospheric pressure, Surf. Coat. Technol. 205 (2011) 3856–3864.
[21] H. Ding, A. Zhu, X. Yang, C. Li, Y. Xu, Removal of formaldehyde from gas streams via packed-bed dielectric barrier discharge plasmas, J. Phys. D. Appl. Phys. 38 (2005) 4160.
[22] Y.C. Hong, H.S. Uhm, W.J. Yi, Atmospheric pressure nitrogen plasma jet: observation of striated multilayer discharge patterns, Appl. Phys. Lett. 93 (2008) 051504.
[23] V.S.-v.d. Gathen, L. Schaper, N. Knake, S. Reuter, K. Niemi, T. Gans, J. Winter, Spatially resolved diagnostics on a microscale atmospheric pressure plasma jet, J. Phys. D. Appl. Phys. 41 (2008) 194004.
[24] B.M. Penetrante, M.C. Hsiao, B.T. Merritt, G.E. Vogtlin, P.H. Wallman, M. Neiger, O. Wolf, T. Hammer, S. Broer, Pulsed corona and dielectric-barrier discharge processing of NO in N2, Appl. Phys. Lett. 68 (1996) 3719–3721.
[25] O. Eichwald, M. Yousfi, A. Hennad, M.D. Benabdessadok, Coupling of chemical kinetics, gas dynamics, and charged particle kinetics models for the analysis of NO reduction from flue gases, J. Appl. Phys. 82 (1997) 4781–4794.
[26] J.T. Herron, Evaluated chemical kinetics data for reactions of N(2D),N(2P), and N2(A3Σu+) in the gas phase, J. Phys. Chem. Ref. Data 28 (1999) 1453–1483.
[27] D. Theirich, C. Soll, F. Leu, J. Engemann, Intermediate gas phase precursors during plasma CVD of HMDSO, Vacuum 71 (2003) 349–359.
[28] R. Atkinson, Kinetics of the gas-phase reactions of a series of organosilicon compounds with hydroxyl and nitrate(NO3) radicals and ozone at 297 ± 2 K, Environ. Sci. Technol. 25 (1991) 863–866.
[29] D. Husain, P.E. Norris, Kinetic study of reactions of ground state silicon atoms, Si[3p2(3P)], by atomic absorption spectroscopy, J. Chem. Soc., Faraday Trans. 2 74 (1978) 106–114.
[30] J.A. Luna-López, G. García-Salgado, T. Díaz-Becerril, J.C. López, D.E. Vázquez-Valerdi, H. Juárez-Santiesteban, E. Rosendo-Andrés, A. Coyopol, FTIR, AFM and PL properties of thin SiOx films deposited by HFCVD, Mater. Sci. Eng. B 174 (2010) 88–92.
[31] R. Reuter, D. Ellerweg, A. von Keudell, J. Benedikt, Surface reactions as carbon removal mechanism in deposition of silicon dioxide films at atmospheric pressure, Appl. Phys. Lett. 98 (2011) 111502.
[32] R. Reuter, N. Gherardi, J. Benedikt, Effect of N2 dielectric barrier discharge treatment on the composition of very thin SiO2-like films deposited from hexamethyldisiloxane at atmospheric pressure, Appl. Phys. Lett. 101 (2012) 194104.
[33] D.G. Howells, B.M. Henry, J. Madocks, H.E. Assender, High quality plasma enhanced chemical vapour deposited silicon oxide gas barrier coatings on polyester films, Thin Solid Films 516 (2008) 3081–3088.
[34] R.N. Tait, T. Smy, S.K. Dew, M.J. Brett, Nodular defect growth and structure in vapor deposited films, J. Electron. Mater. 24 (1995) 935–940.
[35] D. Michael, G. Mirko, T. Sebastian, B. Nikita, A. Peter, Permeation mechanisms of pulsed microwave plasma deposited silicon oxide films for food packaging applications, J. Phys. D. Appl. Phys. 41 (2008) 135207.
[36] H. Chatham, Oxygen diffusion barrier properties of transparent oxide coatings on polymeric substrates, Surf. Coat. Technol. 78 (1996) 1–9.
[37] A.P. Roberts, B.M. Henry, A.P. Sutton, C.R.M. Grovenor, G.A.D. Briggs, T. Miyamoto, M. Kano, Y. Tsukahara, M. Yanaka, Gas permeation in silicon-oxide/polymer (SiOx/PET) barrier films: role of the oxide lattice, nano-defects and macro-defects, J. Membr. Sci. 208 (2002) 75–88.

www.spm.com.cn